Monte Carlo based correction factors for ion chamber dosimetry in heterogeneous phantoms for megavoltage photon beams

Fujio Araki,

Department of Health Sciences, Faculty of Life Sciences, Kumamoto University, 4-24-1 Kuhonji, Kumamoto, Japan

Corresponding Author: Fujio Araki

E-mail: f_araki@kumamoto-u.ac.jp

Telephone number: 81-96-373-5488

Fax number: 81-96-373-5488

Abstract

The purpose of this study was to investigate the perturbation correction factors and inhomogeneity correction factors, ICFs, for a thin-walled cylindrical ion chamber in a heterogeneous phantom including solid water, lung and bone plastic materials. The perturbation factors due to the replacement of the air cavity, non-water equivalence of the wall and the stem, non-air equivalence of the central electrode, and the overall perturbation factor, P_Q, for a cylindrical chamber, in the heterogeneous phantom were calculated with the EGSnrc/Cavity Monte Carlo code for 6 and 15 MV photon beams. The PTW31010 (0.125 cm^3) chamber was modeled with Monte Carlo simulations, and was used for measurements and calculations of percentage depth-ionization PDI or percentage depth-dose PDD. ICFs were calculated from the ratio of the product of the stopping power ratios, SPRs, and P_Q of lung or bone to solid water. Finally, the measured PDIs were converted to PDDs by using ICFs and were compared with those calculated by the Monte Carlo method. The perturbation effect for the ion chamber in lung material is insignificant at 5×5 cm^2 and 10×10 cm^2 fields but the effect need to be considered under conditions of lateral electron disequilibrium with a 3×3 cm^2 field. ICFs in lung varied up to 2% and 4% depending on the field size for 6 MV and 15 MV, respectively. For bone material, the perturbation effects due to the chamber wall and the stem were more significant at up to 3.5% and 1.6% for 6 MV, respectively. ICFs for bone material were approximately 0.945 and 0.940 for 6 MV and 15 MV, respectively. The converted PDDs by using ICFs were in good agreement with Monte Carlo calculated PDDs. The chamber perturbation correction and SPRs should strictly be considered for ion chamber dosimetry in heterogeneous media. This is more important for small field dosimetry in lung and bone materials.

1. Introduction

The current dosimetry protocols (Almond *et al* 1999, IAEA TRS-398 2001, JSMP 2002, Thwaites *et al* 2003) for megavoltage photon beams have been established with ionization measurements in a water phantom. The absorbed dose to water is derived from the measured ionization to air using the ^{60}Co absorbed dose to water calibration factor, $N_{D,w}^{^{60}\mathrm{Co}}$, and the beam quality conversion factor, k_Q. On the other hand, absorbed dose measurements for heterogeneous media such as lung and bone materials have not been sufficiently established and have various problems, unlike measurements in water. First, dosimetric data such as stopping power ratios and mass energy absorption coefficients for heterogeneous media are not given in the dosimety protocols. The perturbation correction factors for ionization chambers in combination with heterogeneous media are also unknown.

Tissue inhomogeneity corrections for megavoltage photon beams are summarized in the AAPM report 85 (Papanikolaou *et al* 2004). The main contents of the report are related to the principles and features of photon inhomogeneity dose calculations for treatment planning systems, TPS, and contain measured benchmark data from work by Rice *et al* (1988a) and by Zhu and Boyer (1990). However, the report does not include dosimetric data like stopping power ratios of heterogeneous media to water and perturbation correction factors for ionization chambers that are necessary for absorbed dose measurements in heterogeneous media. In fact, inhomogeneity corrections for the human body are performed with dose calculation algorithms installed in TPS. Many modern algorithms are based on model-based convolution methods: superposition, anisotropic analytical algorithm AAA, and pencil beam methods using a water kernel (Ahnesjö *et al* 1999, Fogliata *et al* 2007, Ding *et al* 2007a, Knöös *et al* 2006, Mackie *et al* 1985, Van Esch *et al* 2006). Recently, the Voxel Monte Carlo (Fippel 1999, 2004, Fippel *et al* 1999, Fragosa *et al* 2010, Kawrakow *et al* 1996, Kawrakow and Fippel 2000, Kunzler *et al* 2009, Petoukhova *et al* 2010) and Acuros XB (Bush *et al* 2011, Fogliata *et al* 2011a, 2011b, 2011c, 2011d, Han *et al* 2011, Hoffmann *et al* 2011) radiation transport methods considering the atomic compositions of heterogeneous media have become commercially available as more accurate dose calculation algorithms for heterogeneous media.

The beam modeling for algorithms with model-based convolution methods and radiation transport methods is verified by beam data such as percentage depth-doses, dose profiles and output factors measured in a water phantom, and in addition beam data measured in air are also used for the beam modeling of the Monte Carlo method. For clinical application, the dose calculation accuracy of algorithms for the human body that includes heterogeneous media is very important. The human body consists of a variety of tissues and cavities with different physical and radiological properties, which are radiologically different from water, including typically lungs, air, and bones. The dose calculation accuracy of algorithms, however, cannot be verified by direct measurements in the human body. So a phantom with a combination of lung-, water-, and bone-like materials is often used to check the dose calculation accuracy for heterogeneous media (Carrasco *et al* 2004, 2007, Fippel *et al* 1999, Fragoso *et al* 2010, Kunzler *et al* 2009, Petoukhova *et al* 2010, Van Esch *et al* 2006, Zhu *et al* 1990).

Inhomogeneity correction factors, ICFs, in heterogeneous media are generally obtained for lung- and bone-like materials. ICFs are roughly determined as ratios of measured ionizations between heterogeneous and water-like media. This is possible for the lung dose correction under conditions of lateral electron equilibrium (Carrasco *et al* 2004, Fragoso *et al* 2010, Mauceri and Kase 1987, Rice *et al* 1988b). However, ICFs should be considered for lung under conditions of lateral electron disequilibrium (Aspradakis *et al* 2006, Krieger *et al* 2005, Pisaturo *et al* 2012, Rice *et al* 1988b, Ding *et al* 2007b) and for heterogeneous media such as bone with composition different from water (Papanikolaou *et al* 2004, Zhu *et al* 1990). The stopping power ratios to lung, soft tissue, and bone materials have been reported in detail by Siebers *et al* (2000). As mentioned above, the chamber perturbation correction for heterogeneous phantom has been investigated in previous studies but individual correction factors such as the replacement correction factor, P_{repl}, the wall correction factor, P_{wall}, the stem correction factor, P_{stem}, and the central electrode correction factor, P_{cel}, have not been sufficiently estimated, especially in bone material.

The purpose of this study was to investigate each perturbation correction factor and ICFs for a thin-walled cylindrical ion chamber in a heterogeneous phantom including solid water, lung and bone plastic materials. Furthermore, percentage depth-ionization curves measured

with the cylindrical chamber in the heterogeneous phantom were converted to percentage depth-dose curves by using ICFs and were compared with those calculated using the Monte Carlo method.

2. Materials and methods

2.1. Heterogeneous phantom design

The heterogeneous phantom model was made up by 4 layers of solid water (5 cm thickness), lung (5 cm thickness), bone (5 cm thickness), and solid water (10 cm thickness) with a 30×30 cm^2 square slab as shown in figure 1. The heterogeneous plastic phantom (Gammex, RMI, Wisconsin) consists of Solid Water RMI-457 (SW, mass density ρ=1.046 g/cm^3 and relative electron density ρ_e=1.018), LN300 RMI-455 (LUNG, ρ=0.3 g/cm^3, ρ_e=0.293), and Bone SB3 RMI-450 (BONE, ρ=1.819 g/cm^3, ρ_e=1.696). The elemental composition in fraction by weight, mass density, ρ [g/cm^3], electron densities, ρ_e*[el/g] and ρ_e [el/cm^3], for water and the plastic phantoms, the relative electron densities of plastic to water, ρ_e*(*pl*) and ρ_e (*pl*) are presented in tables 1 and 2. ρ_e*[el/g] is calculated by

$$\rho_e^* = \sum_i \frac{N_A w_i Z_i}{A_i}, \qquad (1)$$

where N_A is Avogadro's number, w_i is the fraction by weight of element i, and Z_i and A_i are the atomic number and atomic weight of i, respectively. ρ_e [el/cm^3] is given by

$$\rho_e = \rho_e^* \times \rho \, . \qquad (2)$$

2.2. The perturbation correction factors of an ionization chamber

The perturbation factors for a cylindrical chamber in the heterogeneous phantom were calculated for 6 MV and 15 MV photon beams. The PTW31010 (0.125 cm^3 Semiflex) cylindrical ionization chamber was used for measurements and for Monte Carlo calculations of depth-ionization curves or depth-dose curves with field sizes of 3×3, 5×5, and 10×10 cm^2 at a source-surface distance SSD of 100 cm. Each perturbation factor was obtained from the following equations (Ono *et al* 2010, Yoshiyama *et al* 2010).

$$P_{repl} = (D_m / D_{air}) / (\bar{L} / \rho)^m_{air}, \qquad (3)$$

$$P_{wall} = D_{air} / (D_{air})_{wall}, \qquad (4)$$

$$P_{stem} = (D_{air})_{wall} / (D_{air})_{wall+stem}, \qquad (5)$$

$$P_{cel} = (D_{air})_{wall+stem} / (D_{air})_{chamber}, \qquad (6)$$

$$P_Q = [D_m / (D_{\text{air}})_{\text{chamber}}] / (\bar{L} / \rho)^m_{\text{air}}, \qquad (7)$$

where P_{repl} accounts for the medium of interest being replaced by air in the chamber cavity. P_{wall} corrects the chamber response for the non-medium equivalence of the chamber wall. P_{stem} accounts for the chamber response for the non-medium equivalence of the chamber stem. P_{cel} corrects the chamber response for the effect of the central electrode. P_Q is the overall perturbation factor. Each dose is presented as follows: D_m for medium, D_{air} for air in the chamber cavity, $(D_{\text{air}})_{\text{wall}}$ for air with the chamber wall, $(D_{\text{air}})_{\text{wall+stem}}$ for air with the chamber wall and the stem, and $(D_{\text{air}})_{\text{chamber}}$ for air with the chamber wall, the stem, and the central electrode, as shown in figures 2(a)-(d). $(\bar{L} / \rho)^m_{\text{air}}$ is the average restricted mass collision stopping-power ratio of medium to air. Each dose and $(\bar{L} / \rho)^m_{\text{air}}$ were calculated with EGSnrc (Kawrakow *et al* 2011) user codes Cavity (Kawrakow *et al* 2009) and SPRRZnrc (Rogers *et al* 2011a), respectively, as a function of depths for the heterogeneous phantom shown in figure 1.

To improve the efficiency in the Cavity code, photon splitting was turned on, with a splitting factor of 40 and Russian Roulette for electron that cannot reach the cavity was used with a survival probability of 0.125 (Wulff and Zink 2008). The PTW31010 chamber was modeled with the EGSnrc/Cavity code according to the geometrical dimensions and materials shown in table 3. The chamber stem was modeled with PMMA and a central electrode. The spectra for the incident photon beams were derived from the treatment head simulations for a Varian Clinac iX linear accelerator (Varian Oncology Systems, Palo Alto, CA) using the EGSnrc/BEAMnrc code (Rogers *et al* 2011a, 2011b). The collimated point source was used for the spectrum in the Cavity and SPRRZnrc codes. The dose to medium was calculated with a solid water disc of 0.2 mm thickness and 10 mm diameter as shown in figure 2(a). The adequate disc dimensions are theoretically shown by Kawrakow (2006) for 6 MV and 25 MV photon beams. The point of measurement for the air cavity was taken to be the center of the chamber cavity. Each dose was computed with a statistical uncertainty (1σ) of 0.08%-0.2% depending on the field size and depth. Consequently, their combined uncertainty for each perturbation factor dispersed up to 0.15%-0.3%. The parameters used for simulations were AE=ECUT=521 keV and AP=PCUT=10 keV (Kawrakow (2006).

2.3. Inhomogeneity correction factors for a heterogeneous phantom

The absorbed dose to heterogeneous media D_{inhomo} can be presented according to Spencer-Attix cavity theory by the following equation.

$$D_{\text{inhomo}} = N_{D,w}^{^{60}\text{Co}} \cdot M_{\text{inhomo}} \cdot \frac{[(\bar{L}/\rho)_{\text{air}}^{\text{inhomo}} P_{Q,\text{inhomo}}]_Q}{[(\bar{L}/\rho)_{\text{air}}^{w} P_{Q,w}]_{^{60}\text{Co}}}, \quad (8)$$

where M is the measured ionization and the suffixes inhomo and w represent heterogeneous media and water, respectively. The percentage depth-dose PDD for heterogeneous phantom measurements in figure 1 can be given as follows,

$$\begin{aligned} PDD_{\text{inhomo}}(d,s,f) &= 100 \times \frac{(D_{\text{inhomo}})_d}{(D_{\text{SW}})_{d_{\max}}} \\ &= 100 \times \frac{M_{\text{inhomo},d}}{M_{\text{SW},d_{\max}}} \cdot \frac{[(\bar{L}/\rho)_{\text{air}}^{\text{inhomo}} P_{Q,\text{inhomo}}]_d}{[(\bar{L}/\rho)_{\text{air}}^{\text{SW}} P_{Q,\text{SW}}]_{d_{\max}}}, \end{aligned} \quad (9)$$

where the suffix SW is solid water, d, s, and f are the depth, a field size, and SSD, respectively, and $d_{\max}$ is maximum depth. The percentage depth-ionization PDI and ICF at a depth are defined by the following equations in this study.

$$PDI_{\text{inhomo}}(d,s,f) = 100 \times \frac{M_{\text{inhomo},d}}{M_{\text{SW},d_{\max}}}, \quad (10)$$

$$ICF(d,s) = \frac{[(\bar{L}/\rho)_{\text{air}}^{\text{inhomo}} P_{Q,\text{inhomo}}]_d}{[(\bar{L}/\rho)_{\text{air}}^{\text{SW}} P_{Q,\text{SW}}]_{d_{\max}}}, \quad (11)$$

$$PDD_{\text{inhomo}}(d,s,f) = PDI_{\text{inhomo}}(d,s,f) \cdot ICF(d,s). \quad (12)$$

ICFs were calculated with field sizes of 3×3, 5×5, and 10×10 cm^2 at SSD=100 cm. $d_{\max}$ was 1.5 cm and 3 cm for 6 MV and 15 MV photon beams, respectively. $(\bar{L}/\rho)_{\text{air}}^{m}$ and P_Q for the PTW31010 chamber were obtained from the Monte Carlo calculations described in Sec. 2.2. The uncertainty for ICFs dispersed up to 0.15%-0.3% depending on the field size and depth. Finally, PDI curves measured with the PTW31010 chamber were converted to PDD curves by using ICFs and were compared with those calculated by the EGSnrc/DOSXYZnrc code (Walters *et al* 2011).

3. Results and discussion

3.1. Perturbation factors for a heterogeneous phantom

Perturbation factors for the PTW31010 chamber in a heterogeneous phantom with solid water, lung, and bone slabs are shown as a function of depth for 6 MV and 15 MV photon beams in figures 3(a)-(h). Each perturbation factor for the lung slab agreed with those for

solid water within approximately 0.5% for 5×5 cm^2 and 10×10 cm^2 fields. However, P_{wall} and P_{stem} for lung at a 3×3 cm^2 field were lower than those of other fields because the dose from electrons scattered by the chamber wall or the stem are relatively larger than those from lung due to a lack of lateral electron equilibrium in lung. The tendency became larger for 15 MV because the loss of lateral electron equilibrium increases with higher energy. P_{wall} was 1% and 2% lower than those of solid water at a 3×3 cm^2 field for 6 MV and 15 MV, respectively. P_{stem} showed a similar tendency to P_{wall}. In contrast, P_{repl} for lung at a 3×3 cm^2 field was approximately 1% larger for 6 MV and 15 MV. This is because the electron fluence in the chamber cavity decreases due to a lack of lateral electron equilibrium in lung. P_{cel} for the lung slab was almost independent of the field size and almost the same as that of solid water.

The perturbation factors for bone material differ from those of solid water concerning P_{wall} and P_{stem}. P_{wall} values for bone were larger by up to 3.5% and 2.5% than those for solid water at a 10×10 cm^2 field for 6 MV and 15 MV, respectively. Similarly P_{stem} was approximately l.5% larger for 6 MV and 15 MV. In bone material with a higher atomic number and a higher density, due to its higher angular scattering power, the electrons released would be scattered at wider angles (Carrasco *et al* 2007). Consequently, the dose from electrons scattered by the chamber wall or the stem reduces compared to those from bone material. The effect is larger for 6 MV than for 15MV as shown in P_{wall}. The perturbation factors for bone showed slight field dependence. P_{cel} for bone and lung were almost independent of the field size and almost the same as that of solid water.

3.2. P_Q, SPRs, and ICFs for a heterogeneous phantom

Figures 4(a)-(f) present the overall perturbation factors, SPRs, and inhomogeneity correction factors as a function of depth for 6 MV and 15 MV photon beams. P_Q for solid water was 0.985-0.990, except for the build-up region, and P_Q for lung agreed within 1% for solid water at 5×5 cm^2 and 10×10 cm^2 fields. For a 3×3 cm^2 field, P_Q was 1.5% and 3% lower than those of solid water for 6 MV and 15 MV, respectively, due mainly to perturbation effects of the chamber wall and the stem. P_Q values for bone were 5%-6% and 4% larger than those of solid water for 6 MV and 15 MV, respectively. In addition, P_Q and

SPRs for solid water were 0.5% and 2%~2.5% lower than those of water, respectively. (Seuntjens *et al* 2005) The difference in P_Q is mainly attributable to P_{wall}.

SPRs for lung were approximately 1% and 2% higher than those of solid water for 6 MV and 15 MV, respectively, and were almost independent of the field size. Consequently, ICFs for lung obtained from P_Q and SPRs using equation (11) were 1.01 and 0.99 at 10×10 cm^2 and 3×3 cm^2 fields for 6 MV, respectively, and 1.02 and 0.98 at 10×10 cm^2 and 3×3 cm^2 fields for 15 MV, respectively. Mauceri and Kase (1987) experimentally obtained the perturbation correction to ion chamber measurements in lung. The solid water and lung substitute phantoms that they used had similar elemental composition fractions by weight as those used in present study. They evaluated the perturbation effect for a PTW 0.1 cm^3 cylindrical ion chamber with a thin wall (~0.1 g/cm^2) at a 10×10 cm^2 field. The results demonstrated that the non-medium equivalence of the chamber wall can be ignored, provided that a small, approximately tissue-equivalent, thin-walled ion chamber is used for measuring ICFs in lung. They measured perturbation factors from the ratio of charges collected with the ion chamber in solid water and lung materials and did not consider SPRs for either material. Their results agreed well with values in present study at a 10×10 cm^2 field without the SPR correction.

SPRs for the bone material were approximately 10% lower than those for solid water for 6 MV and 15 MV, and were almost independent of field size. Consequently, ICFs for bone obtained from P_Q and SPRs were 0.95 and 0.94 at 10×10 cm^2 and 3×3 cm^2 fields for 6 MV, respectively, and approximately 0.94 for 15 MV. Zhu and Boyer (1990) calculated ICFs using ratios (bone phantom material to water) of the products of SPR and P_{wall} for a PTW 0.1 cm^3 chamber. ICFs of bone material to water were 0.929 and 0.925 for 6 MV and 18 MV, respectively, and were approximately 2% lower than the values calculated in this study. This is due mainly to the difference in SPRs between solid water and water. It is reported in the AAPM report 85 that ICFs for bone material are more important and thus “raw” ionization readings should not be used directly for bone dosimetry with ion chambers. This study indicated that P_{wall} and P_{stem} for ion chambers and SPRs should be considered for bone material.

Figures 5(a)-(f) show measured PDIs and PDDs and Monte Carlo calculated PDD as a function of depth for 6 MV and 15 MV photon beams. PDIs in lung measured with the PTW31010 chamber differ from calculated PDDs by approximately 1% and 2% for 6 MV and 15 MV, respectively. Measured PDDs in lung obtained by multiplying PDIs by ICFs were in good agreement with the calculated PDDs. PDIs in bone measured with the PTW31010 chamber were 5.3%-6.3% and 6%-7% higher than the calculated PDDs for 6 MV and 15 MV, respectively. Measured PDDs in bone were in good agreement within 1%, with the calculated PDDs. Recently, Fragoso *et al* (2010) compared depth-dose data measured by a PTW pinpoint ion chamber with iPlan XVMC Monte Carlo calculated depth-dose curves in heterogeneous phantoms for 6 MV. The depth-dose data in lung were close to the PDI in present study because the chamber perturbation factors are not considered. For bone material, the PTW pinpoint depth-dose data were also corrected only by SPRs without chamber perturbation factors and thus the measured data were underestimated compared to Monte Carlo calculated depth doses.

4. Conclusions

This study investigated the perturbation correction factors and ICFs for the thin-walled cylindrical ion chamber in the heterogeneous phantom including solid water, lung and bone plastic materials. The perturbation effect in lung material is insignificant under the lateral electron equilibrium but the effect cannot be ignored under conditions of lateral electron disequilibrium. ICFs in lung varied by up to 2% and 4% depending on field size for 6 MV and 15 MV, respectively. For bone material, the perturbation effects due to the chamber wall and the stem become more significant, being up to 3.5% and 1.6% for 6 MV, respectively. As for SPRs, the difference between solid water and lung was within 2% but SPRs of bone material were approximately 10% lower than those of solid water. ICFs for bone material were approximately 0.945 and 0.940 for 6 MV and 15 MV, respectively. PDIs measured with the cylindrical ion chamber in heterogeneous phantoms were converted to PDDs by using ICFs, which were in good agreement with Monte Carlo calculated PDDs. This study indicated that chamber perturbation correction and SPRs should be considered for the ion chamber dosimetry in heterogeneous media.

Acknowledgements

The authors would like to thank Mr. Nakaguchi of Kumamoto University Hospital for performing ion chamber measurements in homogeneity phantoms.

References

Ahnesjö A and Aspradakis M M 1999 Dose calculations for external photon beams in radiotherapy *Phys. Med. Biol.* **44** 99-155

Almond P R, Biggs P J, Coursey B M, Hanson W F, Huq M S, Nath R and Rogers D W, 1999 AAPM's TG-51 protocol for clinical reference dosimetry of high-energy photon and electron beams *Med. Phys.* **26** 1847-70

Aspradakis M M, Mccallum HM and Wilson N 2006 Dosimetric and treatment planning considerations for radiotherapy of the chest wall *Br. J. Radiol.* ***79*** *828-36*

Bush K, Gagne I M, Zavgorodni S, Ansbacher W and Beckham W 2011 Dosimetric validation of Acuros XB with Monte Carlo methods for photon dose calculations *Med. Phys.* **38** 2208-21

Carrasco P, Jornet N, Duch M A, Weber L, Ginjaume M, Eudaldo T, Jurado D, Ruiz A and Ribas M 2004 Comparison of dose calculation algorithms in phantoms with lung equivalent heterogeneities under conditions of lateral electronic disequilibrium *Med. Phys.* **31** 2899-911

Carrasco P, Jornet N, Duch M A, Panettieri V, Weber L, Eudaldo T, Ginjaume M and Ribas M 2007 Comparison of dose calculation algorithms in slab phantoms with cortical bone equivalent heterogeneities *Med. Phys.* **34** 3323-33

Ding G X, Duggan D M, Lu B, Hallahan D E, Cmelak A, Malcolm A, Newton J, Deeley M and Coffey C W 2007a Impact of inhomogeneity corrections on dose coverage in the treatment of lung cancer using stereotactic body radiation therapy *Med. Phys.* **34** 2985-94

Ding G X, Duggan D M and Coffey C W 2007b Comment on “Testing of the analytical anisotropic algorithm for photon dose calculation” [Med. Phys. 33, 4130-4148 82006] *Med. Phys.* **34** 3414

Fippel M 1999 Fast Monte Carlo dose calculation for photon beams based on the VMC electron algorithm *Med. Phys.* **26** 1466-75

Fippel M, W. Laub, Huber B and Nusslin F 1999 Experimental investigation of a fast Monte Carlo photon beam dose calculation algorithm Phys. Med. Biol. **44** 3039-54

Fippel M 2004 Efficient particle transport simulation through beam modulating devices for Monte Carlo treatment planning *Med. Phys.* **31** 1235-42

Fogliata A, Vanetti E, Albers D, Brink C, Clivio A, Knöös T, Nicolini G and Cozzi, L 2007 On the dosimetric behaviour of photon dose calculation algorithms in the presence of simple geometric heterogeneities: comparison with Monte Carlo calculations *Phys. Med. Biol.* **52** 1363-85

Fogliata A, Nicolini G, Clivio A, Vanetti E, Mancosu P and Cozzi L 2011a Dosimetric validation of the Acuros XB Advanced Dose Calculation algorithm: fundamental characterization in water *Phys. Med. Biol.* **56** 1879-904

Fogliata A, Nicolini G, Clivio A, Vanetti E and Cozzi L 2011b Dosimetric evaluation of Acuros XB Advanced Dose Calculation algorithm in heterogeneous media *Radiat. Oncol.* 6 **82**

Fogliata A, Nicolini G, Clivio A, Vanetti E and Cozzi L 2011c On the dosimetric impact of inhomogeneity management in the Acuros XB algorithm for breast treatment *Radiat Oncol.* 6 **103**

Fogliata A, Nicolini G, Clivio A, Vanetti E and Cozzi L 2011d Accuracy of Acuros XB and AAA dose calculation for small fields with reference to RapidArc® stereotactic treatments *Med. Phys*. **38** 6228-37

Fragoso M, Wen N, Kumar S, Liu D, Ryu S, Movsas B, Munther A and Chetty I J 2010 Dosimetric verification and clinical evaluation of a new commercially available Monte Carlo-based dose algorithm for application in stereotactic body radiation therapy (SBRT) treatment planning *Phys. Med. Biol.* **55** 4445-64

Han T, Mikell J K, Salehpour M and Mourtada F 2011 Dosimetric comparison of Acuros XB deterministic radiation transport method with Monte Carlo and model-based convolution methods in heterogeneous media *Med. Phys.* **38** 2651-64

Hoffmann L, Jorgensen M B, Muren L P and Petersen J B 2011 Clinical validation of the Acuros XB photon dose calculation algorithm, a grid-based Boltzmann equation solver *Acta. Oncol.* Posted online on 7 Nov.

IAEA 2001 Absorbed Dose Determination in External Beam Radiotherapy: An International code of practice for dosimetry based standards of absorbed dose to water *Technical Report Series No. 398* (IAEA, Vienna)

JSMP: Japanese Society of Medical Physics 2002 The standard dosimetry of absorbed dose

in external beam radiotherapy *Tsusho-sangyo-kenkyusya, Tokyo* (in Japanese)

Kawrakow I, Fippel M and Friedrich K 1996 3D electron dose calculation using a Voxel based Monte Carlo algorithm (VMC) *Med. Phys.* **23** 445-57

Kawrakow I and Fippel M 2000 Investigation of variance reduction techniques for Monte Carlo photon dose calculation using XVMC *Phys. Med. Biol.* **45** 2163-83

Kawrakow I 2006 On the effective point of measurement in megavoltage photon beams *Med. Phys.* **33** 1829-39

Kawrakow I, Mainegra-Hing E, Tessier F, and Walters B 2009 The EGSnrc C++ class library: EGSnrc C++ user code, Cavity *National Research Council of Canada Report PIRS-898*

Kawrakow I, Mainegra-Hing E, Rogers D W, Tessier F and Walters B 2011 The EGSnrc code system: Monte Carlo Simulation of Electron and Photon Transport *National Research Council of Canada Report PIRS-701*

Knöös T, Wieslander E, Cozzi L, Brink C, Fogliata A, Albers D, Nystrom H and Lassen S 2006 Comparison of dose calculation algorithms for treatment planning in external photon beam therapy for clinical situations *Phys. Med. Biol.* **51**, 5785-807

Krieger T and Sauer O A 2005 Monte Carlo- versus pencil-beam-/collapsed-cone-dose calculation in a heterogeneous multi-layer phantom *Phys. Med. Biol.* **50** 859-68

Kunzler T, Fotina I, Stock M and Georg D 2009 Experimental verification of a commercial Monte Carlo-based dose calculation module for high-energy photon beams *Phys. Med. Biol.* **54** 7363-77

Mackie T R, Scrimger J W and Battista J J 1985 A convolution method of calculating dose for 15-MV x rays *Med. Phys*. **12** 188-96

Mauceri T and Kase K 1987 Effects of ionization chamber construction on dose measurements in a heterogeneity *Med. Phys.* **14** 653-6

Ono T, Araki F and Yoshiyama F 2010 Perturbation correction factors for cylindrical ionization chambers in high-energy electron beams *Radiol. Phys. Technol.* **3** 93-7

Yoshiyama F, Araki F and Ono T 2010 The perturbation correction factors for cylindrical ionization chambers in high-energy photon beams *Radiol. Phys. Technol.* **3** 159-64

Papanikolaou N, Battista J J, Boyer A L, Kappas C, Klein E, Mackie T R, Sharpe M and Dyke J V 2004 Tissue inhomogeneity corrections for megavoltage photon beams *AAPM report No. 85.*

Petoukhova AL , van Wingerden K, Wiggenraad R G, van de Vaart P J, van Egmond J,. Franken E M and van Santvoort J P 2010 Verification measurements and clinical evaluation of the iPlan RT Monte Carlo dose algorithm for 6 MV photon energy *Phys. Med. Biol.* **55** 4601-14

Pisaturo O, Pachoud M, Bochud F O and Moeckli R 2012 Calculation of correction factors for ionization chamber measurements with small fields in low-density media *Phys. Med. Biol.* **57** 4589-98

Rice R K, Mijnheer B J and Chin L M 1988a Benchmark measurements for lung dose corrections for x-ray beams *Int. J. Radiat. Oncol. Biol. Phys.* **15** 399-409

Rice R K, Hansen J L, Chin L M, Mijnheer B J and Bjängard B E 1988b The influence of ionization chamber and phantom design on the measurement of lung dose in photon beams *Med. Phys*. **15** 884-90

Rogers D W, Kawrakow I, Seuntjens J P, Walters B and Mainegra-Hing E 2011a NRC User Codes for EGSnrc *National Research Council of Canada Report PIRS-702* Rev C

Rogers D W, Walters B and Kawrakow I 2011b BEAMnrc Users Manual *National Research Council of Canada Report PIRS-0509* (A) Rev L

Seuntjens J, Olivares M, Evans M and Podgorsak E 2005 Absorbed dose to water reference dosimetry using solid phantoms in the context of absorbed-dose protocols *Med. Phys.* **32** 2945-53

Siebers J V, Keall P J, Nahum A E and Mohan R 2000 Converting absorbed dose to medium to absorbed dose to water for Monte Carlo based photon beam dose calculations *Phys. Med. Biol.* **45** 983-95

Thwaites D I, DuSautoy A R, Jordan T, McEwen M R, Nisbet A, Nahum A E and Pitchford W G 2003 The IPEM code of practice for electron dosimetry for radiotherapy beams of initial energy from 4 to 25 MeV based on an absorbed dose to water calibration *Phys. Med. Biol.* **48** 2929-70

Van Esch A, Tillikainen L, Pyykkonen J, Tenhunen M, Helminen H, Siljamaki S, Alakuijala J, Paiusco M, Lori M and D. P. Huyskens D P 2006 Testing of the analytical anisotropic algorithm for photon dose calculation *Med. Phys.* **33** 4130-48

Walters B, Kawrakow I and Rogers D W 2011 DOSXYZnrc Users Manual *National Research Council of Canada Report PIRS-794* Rev B

Zhu Y and Boyer A L 1990 X-ray dose calculations in heterogeneous media using 3-dimentional FFT convolution *Phys. Med. Biol.* **35** 351-68

Wulff J and Zink K 2008 Efficiency improvements for ion chamber calculations in high energy photon beams *Med. Phys.* **35** 1328-36

Table 1. The elemental comparison in fraction by weight of phantom materials used in the Monte Carlo calculations. The data for plastic materials are provided by Gammex Inc.

Element	Water	RMI457	LN300	RMI450
H	0.1119	0.0802	0.0846	0.0341
C		0.6723	0.5938	0.3141
N		0.0241	0.0196	0.0184
O	0.8881	0.1991	0.1814	0.3650
Mg			0.1119	
Si			0.0078	
Cl		0.0014	0.0010	0.0004
Ca		0.0231		0.2681

Table 2. Mass density, ρ [g/cm^3], and electron densities, ρ_e*[el/g] and ρ_e [el/cm^3], for phantom materials, and the relative electron densities of plastic to water, ρ_e*(pl) and ρ_e(pl). Mass densities for plastic materials are provided by Gammex Inc.

Density	Water	RMI457	LN300	RMI450
ρ [g/cm^3]	0.998[a]	1.046	0.300	1.819
ρ_e*[el/g][b]	3.343×10^{23}	3.247×10^{23}	3.256×10^{23}	3.110×10^{23}
ρ_e*(pl)	1.000	0.971	0.974	0.930
ρ_e [el/cm^3][c]	3.335×10^{23}	3.397×10^{23}	9.768×10^{22}	5.657×10^{23}
ρ_e(pl)	1.000	1.018	0.293	1.696

[a]Mass density for pure water at 22.0 ℃.
[b]ρ_e* is calculated from Eq. (9) in text.
[c]$\rho_e=\rho_e^*\times\rho$

Table 3. Geometrical dimensions and materials of a PTW31010 chamber.

Chamber type	Wall of sensitive volume Total wall of area density	Dimension of sensitive volume	Central electrode
0.125 cm^3 Semiflex	0.55 mm PMMA, 1.19 g/cm^3 0.15 mm graphite, 0.82 g/cm^3 0.078 g/cm^2	radius 2.75 mm length 6.5 mm	aluminium diameter 1.1 mm

Figure captions

Figure 1. The heterogeneous phantom model made up by combining solid water with lung and bone slabs. The chamber moves along depths of a central axis for Monte Carlo calculations of perturbation factors and PDI measurements.

Figure 2. Simplified schematic geometries used to calculate perturbation factors for a PTW 31010 chamber: (a) the dose to medium, D_m, (b) the dose to air in the chamber cavity, D_{air}, (c) the dose to air with the chamber wall, $(D_{air})_{wall}$, (d) the dose to air with the chamber wall and the stem, $(D_{air})_{wall+stem}$, (e) the dose to air with the chamber wall, the stem, and the central electrode, $(D_{air})_{chamber}$. Geometrical dimensions and materials of a PTW31010 chamber are shown in Table III. The point of measurement for the air cavity was taken to be the center of the chamber cavity.

Figure 3. Perturbation factors P_{repl}, P_{wall}, P_{stem}, and P_{cel} for the PTW31010 chamber in a heterogeneous phantom with solid water, lung, and bone slabs. Each perturbation factor is shown as a function of depth at 3×3 cm^2, 5×5 cm^2, and 10×10 cm^2 fields for 6 MV and 15 MV photon beams

Figure 4. Overall perturbation factors P_Q for the PTW31010 chamber, SPRs, and inhomogeneity correction factors ICFs in the heterogeneous phantom. Respective values are shown as a function of depth at 3×3 cm^2, 5×5 cm^2, and 10×10 cm^2 fields for 6 MV and 15 MV photon beams.

Figure 5. PDIs and PDDs measured with the PTW31010 chamber and Monte Carlo calculated PDD in the heterogeneous phantom. PDIs and PDDs are shown as a function of depth at 3×3 cm^2, 5×5 cm^2, and 10×10 cm^2 fields for 6 MV and 15 MV photon beams.

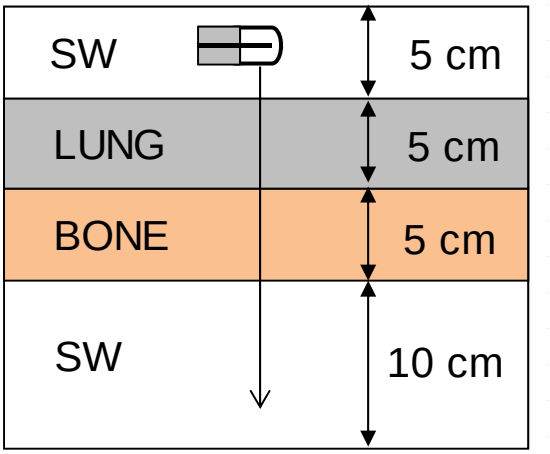

Figure 1. The heterogeneous phantom model made up by combination solid water with lung and bone slabs. The chamber moves along depth of a central axis for Monte Carlo calculations of perturbation factors and PDI measurements.

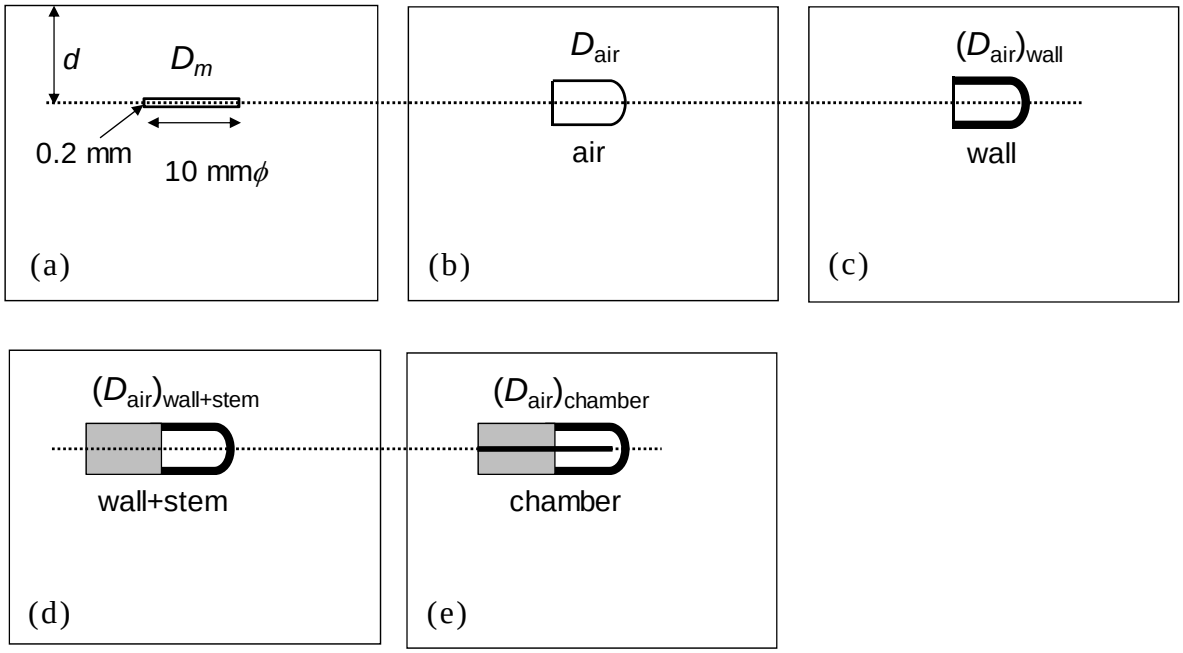

Figure 2. Simplified schematic geometries used to calculate perturbation factors for a PTW 31010 chamber: (a) the dose to medium, D_m, (b) the dose to air in the chamber cavity, D_{air}, (c) the dose to air with the chamber wall, $(D_{air})_{wall}$, (d) the dose to air with the chamber wall and the stem, $(D_{air})_{wall+stem}$, (e) the dose to air with the chamber wall, the stem, and the central electrode, $(D_{air})_{chamber}$. Geometrical dimensions and materials of a PTW31010 chamber are shown in table 3. The point of measurement for the air cavity was taken to be the center of the chamber cavity.

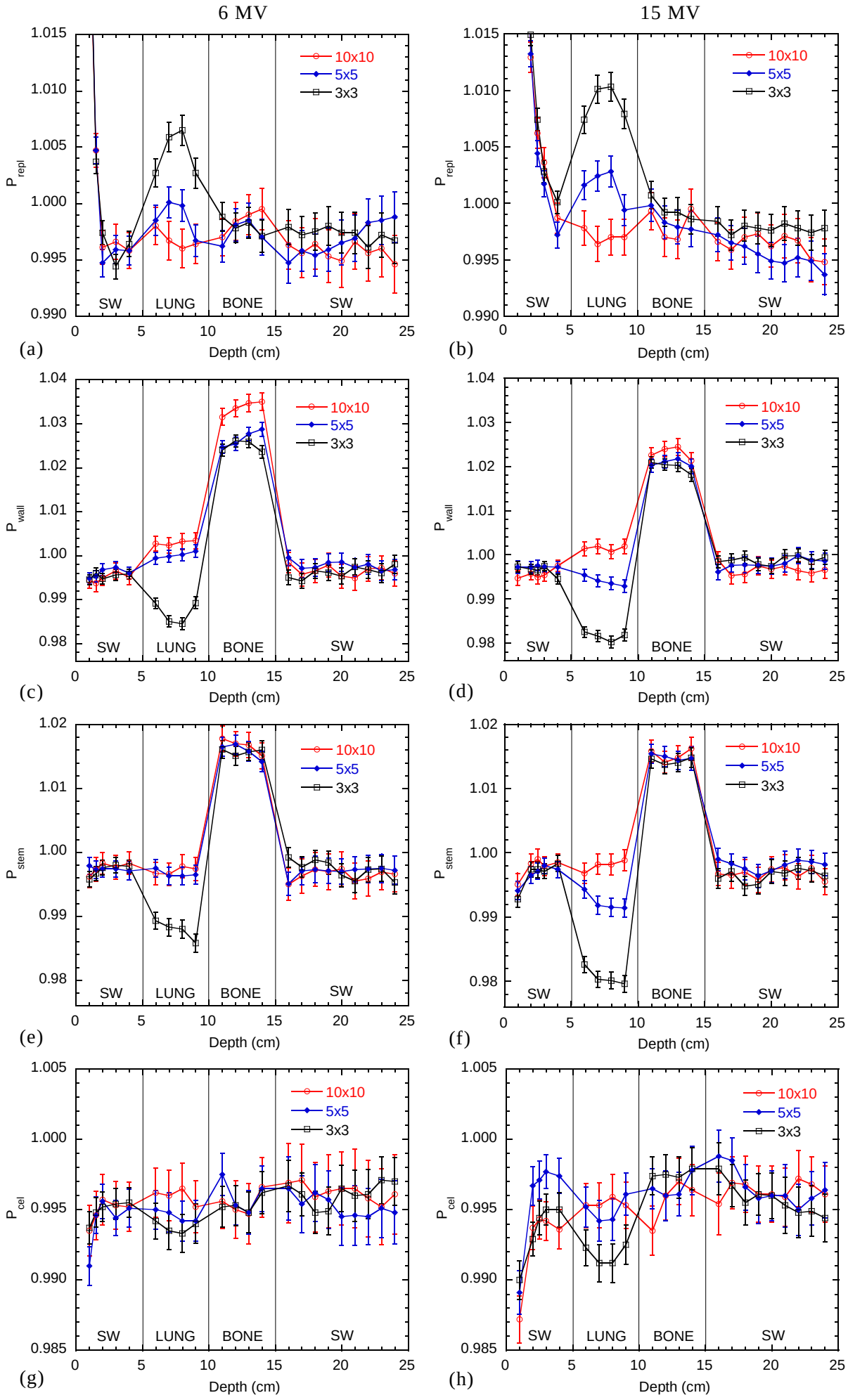
6 MV
15 MV
10x10
5x5
3x3
SW
LUNG
BONE
SW
Depth (cm)
P repl
P wall
P stem
P cel
(a)
(b)
(c)
(d)
(e)
(f)
(g)
(h)

Figure 3. Perturbation factors P_{repl}, P_{wall}, P_{stem}, and P_{cel} for the PTW31010 chamber in a heterogeneous phantom with solid water, lung, and bone slabs. Each perturbation factor is shown as a function of depth at 3×3 cm^2, 5×5 cm^2, and 10×10 cm^2 fields for 6 MV and 15 MV photon beams.

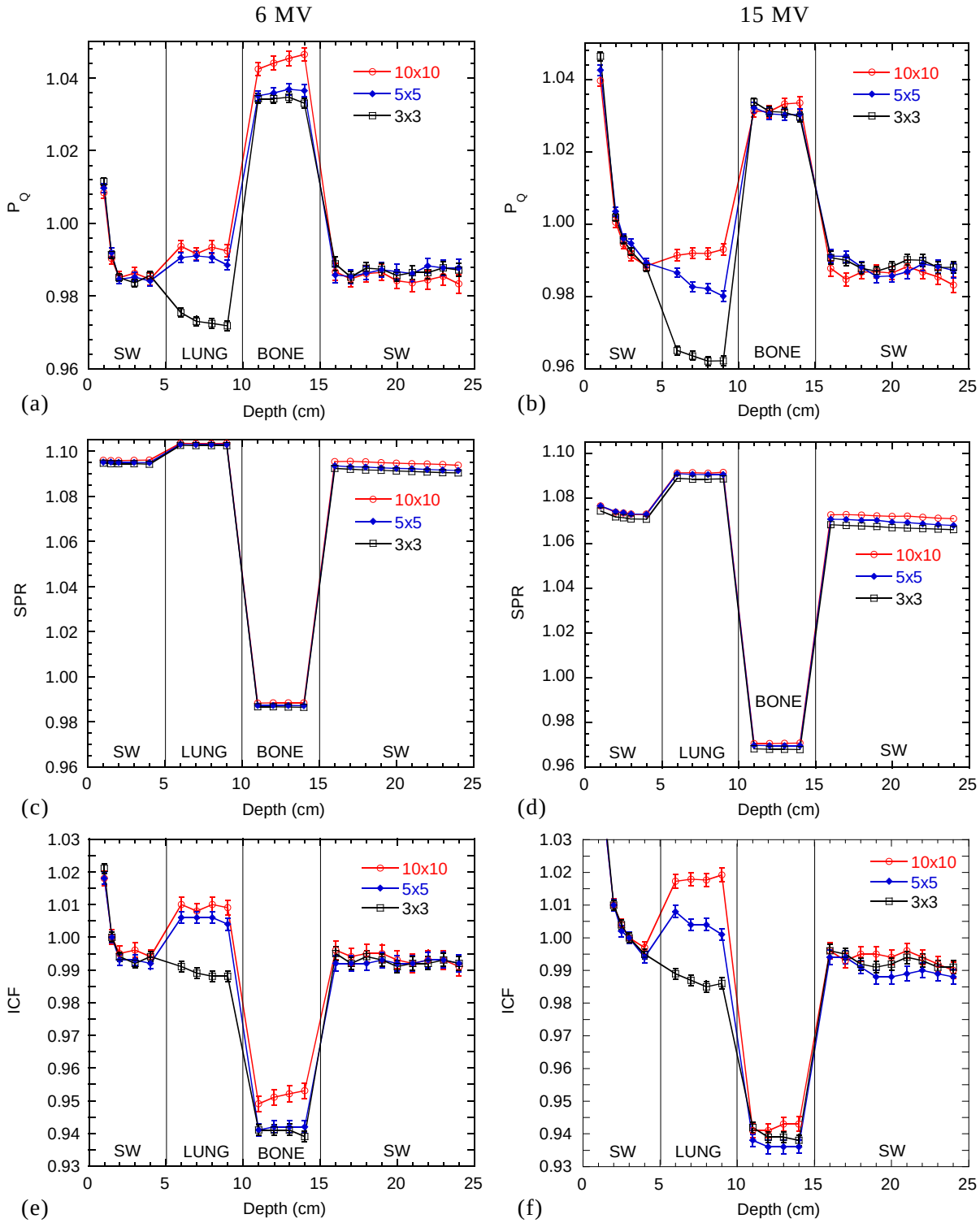

Figure 4. Overall perturbation factors P_Q for the PTW31010 chamber, SPRs, and inhomogeneity correction factors ICFs in a heterogeneous phantom. Respective values are shown as a function of depth at 3×3 cm^2, 5×5 cm^2, and 10×10 cm^2 fields for 6 MV and 15 MV photon beams.

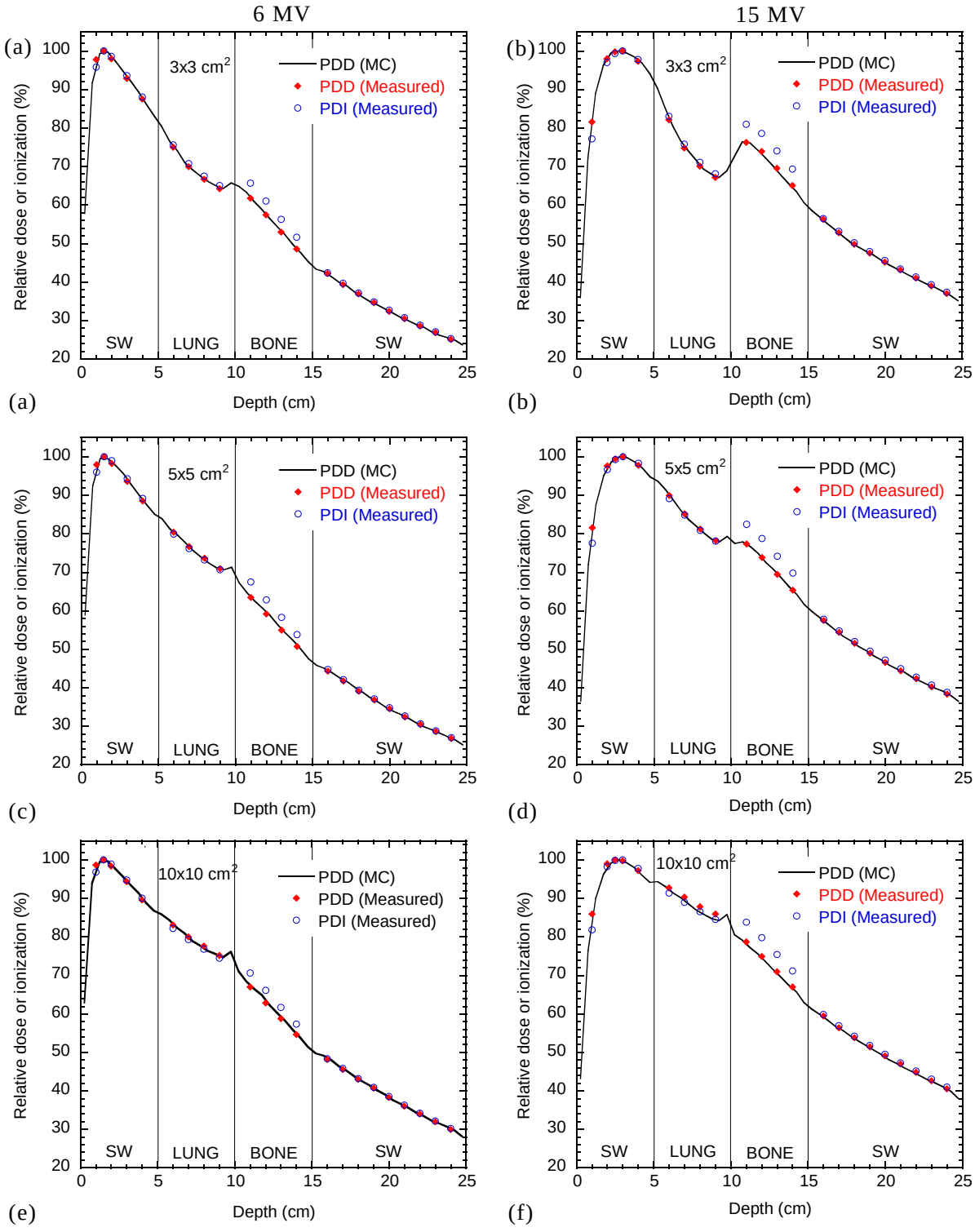

Figure 5. PDIs and PDDs measured with the PTW31010 chamber and Monte Carlo calculated PDD in heterogeneous phantom Model 3. PDIs and PDDs are shown as a function of depth at 3×3 cm^2, 5×5 cm^2, and 10×10 cm^2 fields for 6 MV and 15 MV photon beams.